# Novel Shallow Junction Technology using Decaborane ($B_{10}H_{14}$)

K. Goto, J. Matsuo*, T. Sugii, H. Minakata, I. Yamada*, and T. Hisatsugu

Fujitsu Laboratories Ltd.
10-1 Morinosato-Wakamiya, Atsugi 243-01, Japan

*Ion Beam Engineering Experimental Lab., Kyoto University
Sakyo, Kyoto 606-01, Japan

## Abstract

We have developed the first ever low- energy, high-dosage boron ion implantation technology using a decaborane ($B_{10}H_{14}$) molecule. Since $B_{10}H_{14}$ consists of ten boron atoms, they are implanted with about a one-tenth lower effective acceleration energy and a ten times higher effective beam current compared with those of boron. Using this implantation, we achieved an ultra-shallow 39-nm-deep junction with 1.5 kΩ/sq. To demonstrate the effect and feasibility for semiconductor devices, we have fabricated a high-performance 0.15-μm PMOS device with excellent resistance to short-channel effects.

## Introduction

As MOSFET scaling advances to 0.1-μm, ultra-shallow junctions with low sheet resistance are strongly required for both source/drain extensions and deep regions to suppress the short channel effects while keeping a high current drive ability. Ion implantation technology is widely used for fabricating semiconductor devices. For the deep submicron region, however, it becomes difficult to form a shallow junction by ion implantation, especially for $B^+$ implantation which requires an acceleration energy of less than 1 keV and 5 keV for extension and deep junctions, respectively. Such low energy conditions cause a drastic reduction in the available beam current as defined by the Langmir-Child law (Figure 1). Recently, $BF_2^+$ has been used since it can realize a shallower junction. However, it causes a boron penetration problem due to the existence of fluorine [1]. As an alternative to the ion implantation technology, solid phase diffusion technology has been studied [2]. Considering the CMOS process, however, it causes further complication of the fabrication process, such as requiring two types of side wall for PMOS and NMOS.

In this work, we have developed a low-energy, high-dosage boron ion implantation technology using a decaborane ( $B_{10}H_{14}$) molecule for the first time. Since $B_{10}H_{14}$ consists of

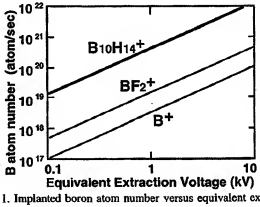


Figure 1. Implanted boron atom number versus equivalent extraction voltage estimated by the Langmir-Child law.

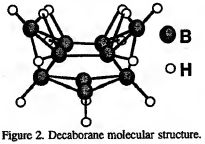


Figure 2. Decaborane molecular structure.

ten boron atoms, it can be implanted with about a one-tenth lower effective acceleration energy and a ten times higher effective beam current compared with those of $B^+$ (Figure 1). In order to demonstrate the effects and practicability of $B_{10}H_{14}^+$ implantation for semiconductor devices, we fabricated a high-performance 0.15-μm PMOS device.

## $B_{10}H_{14}$ ion implantation

Figure 2 shows the molecular structure of decaborane ($B_{10}H_{14}$; 99.7°C melting point; 213°C boiling point at 1 atm) which is a stable solid at room temperature. It is also nontoxic and safer than diborane ($B_2H_6$) which is widely used for semiconductor processes. A sublimation gas of $B_{10}H_{14}$ was introduced into an implantation chamber and ionized by electron



0-7803-3393-4 $5.00 © 1996 IEEE

beam irradiation. The electron beam energy was optimized to prevent the fragmentation of $B_{10}H_{14}$ molecular. Then the $B_{10}H_{14}$ ions were accelerated and implanted into a Si wafer.

## Results and Discussion

### *A. Profile and sheet resistance of Boron atoms*

Figure 3 shows the boron profiles of $B^+$, $BF_2^+$, and $B_{10}H_{14}^+$ implantation at the same acceleration energy of 5 keV. In order to get the same B dosage, implanted dosages of $B^+$, $BF_2^+$, and $B_{10}H_{14}^+$ were set at 1e14, 1e14, and 1e13 ions/cm$^2$, respectively, because $B_{10}H_{14}^+$ has ten B atoms. $B_{10}H_{14}^+$ showed the shallowest boron profile, since the equivalent implantation energy of boron in $B_{10}H_{14}^+$ is smaller than that in $B^+$ and $BF_2^+$. The equivalent implantation energy for B in $B_{10}H_{14}^+$ is calculated to be 0.089 and 0.395 times smaller than that in $B^+$ and $BF_2^+$, respectively.

We investigated the boron diffusion profiles of $B_{10}H_{14}^+$ and $BF_2^+$ implanted as shown in Figure 4 and 5. After implanting at the same condition shown in Figure 3, wafers were subjected to a rapid thermal anneal (RTA) process at 900 °C and 1000 °C for 10 seconds. The boron diffusion of $B_{10}H_{14}^+$ at 900 °C was strongly suppressed compared with that of $BF_2^+$, despite the steeper as-implanted profile of $B_{10}H_{14}^+$ implantation. In addition, the boron profiles of $B_{10}H_{14}^+$ did not show a tail in the low concentration region below 1e18/cm$^2$, which is explained by transient diffusion [3]. It is considered that the damage by $B_{10}H_{14}^+$ implantation is different from that of $BF_2^+$, because $BF_2^+$ has two fluorine atoms per one boron though $B_{10}H_{14}^+$ has just one or two hydrogen atoms, and moreover $B_{10}H_{14}^+$ is implanted as a cluster. This difference of damage may suppress the boron transient diffusion. Annealing at 1000 °C, the boron profile of $B_{10}H_{14}^+$ implantation diffused well in the high concentration region and showed an ideal box shape which may reduce the sheet resistance in the limited junction depth.

Sheet resistances with varying RTA conditions from 900°C to 1050°C for 10 seconds were investigated as shown in Figure 6. Of all the annealing temperature conditions, the sheet resistance of $B_{10}H_{14}^+$ implanted at 5 keV and 10 keV showed resistance as low as $BF_2^+$. This indicates that a $B_{10}H_{14}^+$ implanted wafer is also electrically activated and can reduce the resistance. $B_{10}H_{14}^+$ implanted at 10 keV showed a lower sheet resistance than $BF_2^+$ at 5 keV, though both effective implantation energies were almost the same. It was

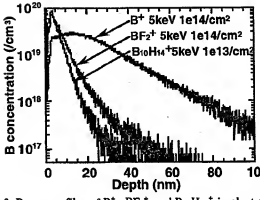


Figure 3. Boron profiles of $B^+$, $BF_2^+$, and $B_{10}H_{14}^+$ implantation.

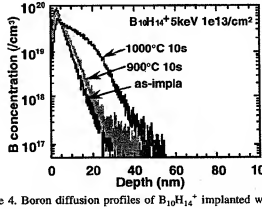


Figure 4. Boron diffusion profiles of $B_{10}H_{14}^+$ implanted wafer after RTA process.

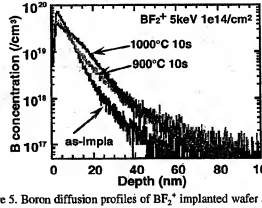


Figure 5. Boron diffusion profiles of $BF_2^+$ implanted wafer after RTA process.

considered that the boron activation rate of $B_{10}H_{14}^+$ implanted wafer might be higher than that of $BF_2^+$, since there is no fluorine which may prevent boron activation. The sheet resistance and junction depth defined at the channel concentration 3e17/cm$^3$ of our fabricated PMOSFET are summarized in Figure 7. The $B_{10}H_{14}^+$ implanted wafer showed a lower sheet resistance while keeping the shallow junction than that of $BF_2^+$, and achieved a 27-nm deep junction with 2.7 kΩ/sq and a 39-nm

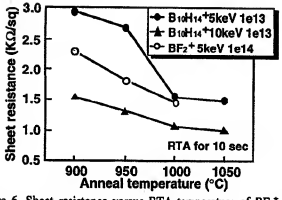


Figure 6. Sheet resistance versus RTA temperature of $BF_2^+$, and $B_{10}H_{14}^+$ implanted wafers.

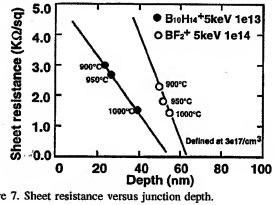


Figure 7. Sheet resistance versus junction depth.

deep junction with 1.5 kΩ/sq. The sheet resistance of the $BF_2^+$ implanted wafer showed a strong dependence on the junction depth due to the existence of tails. Thus, $BF_2^+$ implantation cannot realize shallow junctions with a low enough sheet resistance.

### *B. Device application*

We then demonstrated the feasibility of $B_{10}H_{14}^+$ implantation technology for semiconductor devices. First, we examined the electrical characteristics of pn-junctions formed by $B_{10}H_{14}^+$ implantation. As shown in Figure 8, the pn-junction formed by $B_{10}H_{14}^+$ implantation shows reverse bias characteristics as good as the conventional $BF_2^+$ implanted junction. Next, we fabricated deep submicron devices. Figures 9 and 10 show the device structure and the process steps for the PMOSFETs with a gate length down to 0.1-μm. After a conventional LOCOS process, a 4-nm-thick gate oxide and poly-Si were deposited. To compare the short channel effects, shallow extension regions were formed by $B_{10}H_{14}^+$ or $BF_2^+$ implantation, with the same energy of 5 keV at the effective doses of 1e13 ions/cm$^2$ or 1e14 ions/cm$^2$, respectively. After sidewall formation, deep source/drain junctions and gate

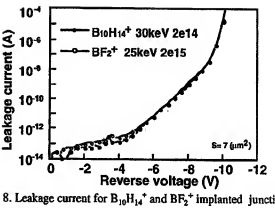


Figure 8. Leakage current for $B_{10}H_{14}^+$ and $BF_2^+$ implanted junctions.

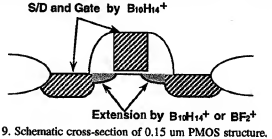


Figure 9. Schematic cross-section of 0.15 um PMOS structure.

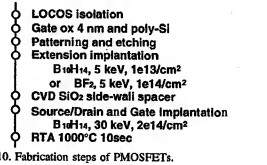


Figure 10. Fabrication steps of PMOSFETs.

regions were simultaneously implanted by $B_{10}H_{14}^+$ with 30 keV at 2e14 ions/cm$^2$. Then a ten second RTA at 1000 °C was performed to activate the implanted impurities.

Figure 11 shows the Id-Vds characteristics of a 0.15-μm PMOSFET with $B_{10}H_{14}^+$ implanted in all of the regions, extensions, source/drain, and gate. An excellent current drive of 0.33 mA/μm was obtained with a threshold voltage of -0.13 V at a supply voltage of -2 V. A good subthreshold swing of 83 mV/dec was also achieved, as shown in Figure 12. These results clearly indicate the practicality of $B_{10}H_{14}$ ion implantation for semiconductor devices as well as B and $BF_2$.

Figures 13 and 14 show the dependence of the threshold voltage on the gate length and the subthreshold swing of PMOSFETs with $B_{10}H_{14}^+$ or $BF_2^+$ implanted in the extension regions. The short-channel effects were suppressed by the $B_{10}H_{14}^+$ implanted extension because the ultra-shallow junction was provided. Figure 15 shows the relationship between Vth

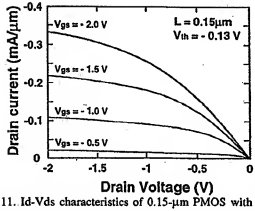


Figure 11. Id-Vds characteristics of 0.15-μm PMOS with $B_{10}H_{14}^+$ implanted extensions.

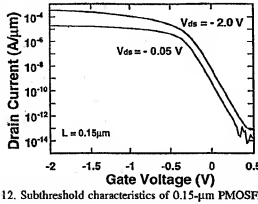


Figure 12. Subthreshold characteristics of 0.15-μm PMOSFET with $B_{10}H_{14}^+$ implanted extensions.

and drain current. No current degradation was observed, when using the $B_{10}H_{14}^+$ implantation technology.

## Conclusion

We applied $B_{10}H_{14}$ ion implantation to semiconductor devices for the first time. This provides us with a low-energy, high-current ion implantation technology. By using this implantation, ultra-shallow junctions were achieved without transient diffusion. We fabricated 0.15-μm PMOSFETs with good current drive ability and excellent resistance to short-channel effects. Experimental data revealed that $B_{10}H_{14}$ ion implantation can be applicable for semiconductor device processes as well as the usual B and $BF_2$ ion implantation, and especially can be more suitable for deep submicron devices.


## Acknowledgments

We thank M. Kase, S. Kawamura of Fujitsu for their discussion. We also thanks D. Takeuchi, N. Shimada of Kyoto Univ. for their help with implantation, and Y.Tada and U. Kataoka of Fujitsu Lab. for SIMS analysis.


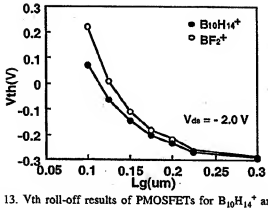


Figure 13. Vth roll-off results of PMOSFETs for $B_{10}H_{14}^+$ and $BF_2^+$ implanted extensions.

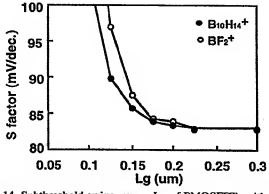


Figure 14. Subthreshold swing versus Lg of PMOSFETs with $B_{10}H_{14}$ and $BF_2^+$ implanted extensions.

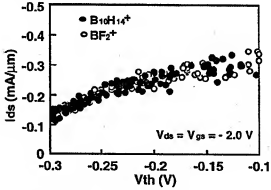


Figure 15. Ids versus Vth of PMOSFETs with $B_{10}H_{14}^+$ and $BF_2$ implanted extensions.

## References


[1] T. Aoyama, K. Suzuki, H. Tashiro, Y. Tada, et al., J. Appl Phys., vol. 77 (1), p. 417, 1995.

[2] K. Takeuchi, T. Yamamoto, A. Furukawa, T. Tamura and K. Yoshida, Symp. on VLSI Tech. Dig, p. 9, 1995.

[3] N. E. B. Cowern, K. T. F. Janssen, and H. F. F. Jos, J Appl. Phys., vol. 68 (12), p. 6191, 1990.